Journal of Theoretical and Applied Physics (2017) 11:301–312
https://doi.org/10.1007/s40094-017-0271-y

RESEARCH

A pulsed plasma jet with the various Ar/N_2 mixtures

A. Barkhordari[1] · A. Ganjovi[1] · I. Mirzaei[1] · A. Falahat[2] · M. N. Rostami Ravari[2]

Received: 23 August 2017 / Accepted: 25 November 2017 / Published online: 9 January 2018

Abstract
In this paper, using the Optical Emission Spectroscopy technique, the physical properties of a fabricated pulsed DBD plasma jet are studied. Ar/N_2 gaseous mixture is taken as operational gas, and Ar contribution in Ar/N_2 mixture is varied from 75 to 95%. Through the optical emission spectra analysis of the pulsed DBD plasma jet, the rotational, vibrational and excitation temperatures and density of electrons in plasma medium of the pulsed plasma jet are obtained. It is seen that, at the wavelength of 750.38 nm, the radiation intensity from the Ar 4p → 4 s transition increases at the higher Ar contributions in Ar/N_2 mixture. It is found that, for 95% of Ar presence in the mixture, the emission intensities from argon and molecular nitrogen are higher, and the emission line intensities will increase nonlinearly. In addition, it is observed that the quenching of Ar^* by N_2 results in the higher intensities of N_2 excited molecules. Moreover, at the higher percentages of Ar in Ar/N_2 mixture, while all the plasma temperatures are increased, the plasma electron density is reduced.

Keywords Pulsed plasma jet · Optical emission spectroscopy · Ar/N_2 gaseous mixture

Introduction

In recent years, the cold atmospheric pressure plasma jets have attracted much attention in the various fields of science and technological applications [1–9]. Plasma discharges at the atmospheric pressures are practically used owing to their simplicity and low manufacturing cost [10]. To have an optimized efficiency of the plasma jet for material processing, cold plasma with the various mixtures of atomic and molecular gases is always applied. Furthermore, the plasma jets with Ar/N_2 gaseous mixture are widely used in different fields of medical applications. These are mainly including skin regeneration owing to its painless effects, wound healing, sterilization and decontamination of medical instruments, etc. [11].

In an experimental work, Khan et al. [12] investigated the basic plasma discharge features of an RF plasma discharge medium with the Ar/N_2 gaseous mixture at the low pressures. They found that the electron temperature is maximized at about 1.8 eV. In addition, at the lower argon percentages in Ar/N_2 mixture, the electron temperature was decreased. Moreover, Qayyum et al. [13] used the optical emission spectroscopic (OES) scheme to analyze the physical features of a Ar/N_2 gaseous mixture plasma discharge with a 50 Hz pulsing power source in a parallel plate structure of metal electrodes. The input power was varied between 175 and 225 W, and the filling pressure was kept between 7 and 9 mbar. They observed that, the molecular nitrogen emission lines intensity and plasma temperature will increase at the higher argon contribution in Ar/N_2 mixture.

Bousquet et al. [14] estimated the plasma physical features of the plasma jet with Ar/N_2 mixture in a reactive magnetron sputtering using the OES method. It was found that, at the higher Ar contributions in the Ar/N_2 mixture, the electron temperature decreases. Kilianova et al. [15] calculated the temperature of different species in a discharge plasma created by helical cavity coupled RF with Ar/N_2 gaseous mixture using the OES measurement scheme. The argon percentage in Ar/N_2 mixture was varied from 0 to 90%. It was shown that, at the lower argon contributions in the mixture, the electron temperature decreases. Additionally, a direct relation between the plasma emission intensity and electron temperature was introduced.

✉ A. Ganjovi
Ganjovi@kgut.ac.ir

[1] Photonics Research Institute, Graduate University of Advanced Technology, Kerman, Iran

[2] Faculty of Physics, Shahid Bahonar University of Kerman, Kerman, Iran

Ohata [16] studied the spectroscopic properties and analytical capability of inductively coupled plasma (ICP) with the Ar/N_2 gaseous mixture using the axial view of OES technique. The emission intensity and excitation temperature were obtained. In addition, it was shown that the electron temperature increases at the higher nitrogen gas flow rates.

Doronin et al. [17] analyzed the luminescence spectroscopic features of a supersonic jet with the nitrogen clusters (containing nearly 100 molecules per cluster) and Ar/N_2 clusters (250 and 400 particles per cluster). For the Ar/N_2 clusters, the main transitions to the different vibrational levels of the ground state from single N_2 molecules in the argon medium were detected. Furthermore, it was observed that, generally, the emission lines of nitrogen atomic ions lie between the wavelengths of 140 and 220 nm.

Generally, the OES technique is an emissive spectroscopy method and it is often applied to determine the physical properties of reactive species in different plasma discharges media, where the other measurement methods are not applicable. Moreover, owing to its non-invasive character of measurements, it can monitor the changes in the nature of the different formed species inside the plasma discharge medium in real time. Therefore, in this paper, the OES technique is used as to determine the different formed species in a developed pulsed DBD plasma jet with the various Ar/N_2 gaseous mixtures. The percentage of argon in Ar/N_2 mixture is varied, and the plasma electron density, rotational, vibrational and excitation temperatures are calculated by analyzing the obtained optical emission spectra from the discharge medium of the pulsed DBD plasma jet.

Experimental setup

Figure 1 shows the schematic representation of the whole experimental setup with the typical view of the designed pulsed plasma jet, gas mixer and spectrometer. As shown, for the designed pulsed DBD plasma jet, both the central tungsten pin (inner) and copper layer (outer) electrodes are powered with the applied impulse voltage. The inner electrode is made of a 1.6 mm diameter and 100 mm length tungsten rod, while its tip sharpened with 30°. The outer electrode is made of a copper layer with inner and outer diameters of 6 and 7 mm, respectively. The length of copper layer is 20 mm. To achieve a uniform positive corona, the inner and outer electrodes are connected to the positive and negative poles, respectively. Moreover, to provide a cold DBD plasma discharge between the inner and outer electrodes, the outer electrode is covered by a quartz tube. The inner and outer diameters and length of quartz tube are 4, 6 and 80 mm, respectively. In addition, this device is able to operate at atmospheric pressures with different gaseous mixtures of argon and nitrogen. Thus, the plasma discharge is formed in a 10 mm gap between the inner and outer electrodes. The length of generated pulsed plasma plume is about 35 mm along the inner electrode. This arrangement for pulsed plasma jet strongly prevents arcing between the inner and outer electrodes. Hence, it is suitable for the biomedical applications. Furthermore, a pulsed power supply is used with variable voltages between 1 and 5 kV and frequencies from 3 to 50 kHz, respectively. The OES measurements are performed by a CCD spectrometer. Argon is taken as the main carrier gas and, it is mixed at different percentages with the molecular nitrogen using a gas mixer. However, the pulsed input power depends on the working gas and dimensions of the pulsed plasma jet electrodes. A 500 kΩ blocking resistance is placed between the positive pole and tungsten electrode. By introducing $(Ar + N_2)$ into the tube, plasma and gas are spewed out from its nozzle, generating a plasma jet at the atmospheric pressure. A 3D schematic representation of the developed DC pulsed DBD plasma jet is shown in Fig. 2.

In this work, the emission spectra of the manufactured pulsed plasma jet are obtained using a USB2000 Oceanoptic Spectrometer. Its fiber probe was placed perpendicularly at 5 mm away from the plasma jet plume. The OES analysis is performed by a Spectrasuite software. It has a linear CCD and spectral resolution of 0.035 nm. Moreover, it saves a full spectrum at every millisecond with a wavelength range sensitivity of 200–1100 nm. In this experimental study, using the OES technique, the excitation, vibrational and rotational temperatures and electron density in the plume of the developed DC-pulsed DBD plasma jet are calculated. It must be noted that, in the non-equilibrium plasma discharges, the following relation usually governs: $T_e > T_{el} > T_v > T_r$. When one or more of four temperatures are not the same, the system has to be considered in non-equilibrium or in partial local thermodynamic equilibrium (PLTE) conditions. In the performed experiments, the developed pulsed DBD plasma jet is in PLTE conditions, where the Maxwell–Boltzmann equilibrium was established. The emission lines from the excited argon species are the Overabundant, and these states have reliable transition probabilities that are published in the literature. Assuming that the upper levels of the selected atomic transitions are in the PLTE conditions, the conventional Boltzmann plot technique can be used to obtain the temperatures in the plume of the pulsed DBD plasma jet.

Tendero et al. noted that, when the plasma electron density and temperature lie between $10^{12} - 10^{16}\mathrm{cm}^{-3}$ and $0.5 - 2\,\mathrm{eV}$, respectively, the plasma discharge is in PLTE [18]. Moreover, Calzada et al. introduced a criterion to determine the plasma equilibrium conditions [19, 20]. The

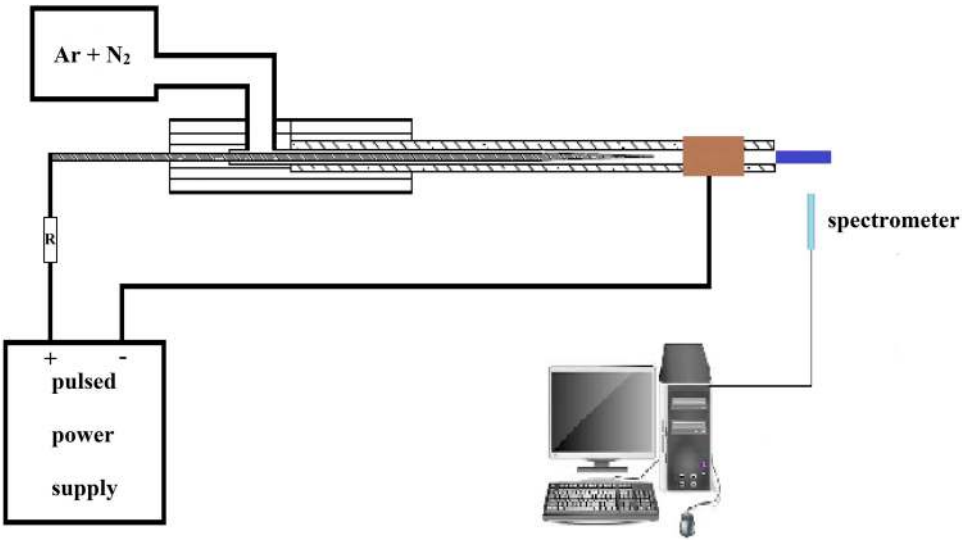

Fig. 1 The schematic representation of the experimental setup

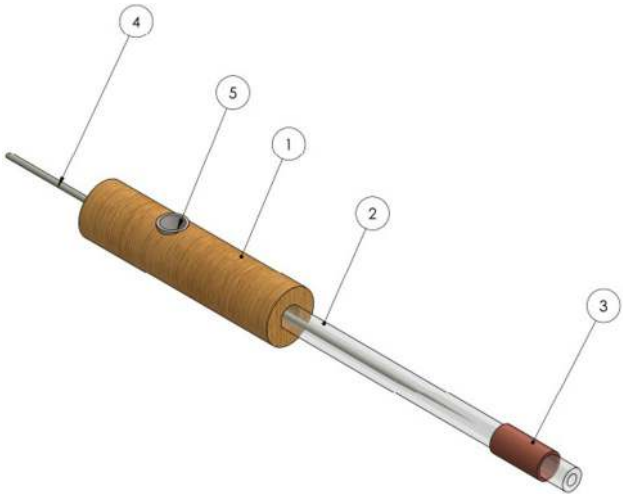

Fig. 2 3D view of the pulsed plasma jet

main hypothesis behind their theory was to consider the atoms as hydrogenic ions with core z ($z = 1$ for neutral atoms; $z = 2$ for single charged ions, etc.). However, the results can be applied to the more complex systems such as He, Ar, etc. Moreover, a Maxwellian distribution function was considered for the electron energy. For a hydrogenic ion, each level will be determined by an effective principal quantum number as follows:

$$P = z\left(\frac{E_H}{E_p}\right)^{1/2} \tag{1}$$

where E_H is the Rydberg constant or hydrogen ionization energy, and E_p is the ionization energy of this level. On the other hand, an index of the equilibrium separation for each level p is defined as follows:

$$b(p) = \frac{n(p)}{n_{\mathrm{SB}}(p)} = \frac{n(p)/g(p)}{n_{\mathrm{SB}}(p)/g(p)} = \frac{\eta(p)}{\eta_{\mathrm{SB}}(p)} \tag{2}$$

where $n(p)$ and $n_{\mathrm{SB}}(p)$ are the real and Saha–Boltzmann equilibrium population, respectively, and $g(p)$ is the statistical weight. The Saha–Boltzmann population equals to:

$$n_{\mathrm{SB}}(p) = n^+ n_e \frac{g(p)}{2g^+}\left(\frac{h^2}{2\pi m_e k T_e}\right)^{3/2} \exp\left(\frac{E_p}{kT_e}\right) \tag{3}$$

where n^+ is the ground state population of the plasma discharge species with charge core $z + 1$, and g^+ is its statistical weight. Moreover, $n_{\mathrm{SB}}(p)$ is equal to the electron density which is obtained from the experimental data for the Stark broadening of the H_β line (486.132 nm). If $b(p) = 1$ for all levels, the ground level is included in the calculations and the plasma discharge will be in the complete LTE. On the other hand, if such a parameter only equals to the unit for a group of levels, then the plasma discharge will be found in PLTE. Moreover, when $b(p) > 1$, the levels will be overpopulated with respect to the Boltzmann equilibrium population (plasma is in the ionization stage). Finally, when $b(p) < 1$, the levels will be underpopulated with respect to the Saha–Boltzmann equilibrium population (plasma is in the recombination stage). Hence, with the obtained electron density from the experiment, $b(p) < 1$, and the plasma discharge is in PLTE [19, 20].

A photograph of the developed pulsed DBD plasma jet in the operational conditions is shown in Fig. 3. The operational parameters of pulsed DBD plasma jet are fixed at the applied voltage of 4.8 kV and frequency of 48 kHz. It appears to be uniform and its length can even reach more than 30 mm. The Ar/N_2 gaseous mixture is injected into the pulsed DBD plasma jet by flow rate of about 15, 1–5

SLM (standard liters per minute), respectively, which is controlled by a velocity flow controller.

Here, the operational features of the fabricated pulsed DBD plasma jet are studied in two different working conditions: (1) the applied pulsed voltage amplitude of 4.8 kV, and frequency and Ar/N_2 ratio are varied between 3 and 48 kHz (by step of 6 kHz) and 3–19, respectively, (2) the applied pulsed frequency is fixed at 48 kHz, and the voltage and Ar/N_2 ratio are varied between 3 and 4.8 kV (by step of 0.2) and 3–19, respectively.

Analysis of results

The electron collisions excite the plasma species to the higher atomic or molecular levels decaying and emitting photon at the specific wavelengths. These processes can be detected and analyzed by recording the emission spectra. To determine the various reactive species generated in the Ar/N_2 pulsed plasma jet and to calculate its operational parameters, the OES technique is applied to record the emission spectra of the jet. As seen in Fig. 4, the two typical emission spectra are recorded at the pulsed DBD plasma jet plume. These emission spectra are recorded at two different argon percentages in the mixture, i.e. 70 and 95%, applied voltage and frequency of 4.8 kV and 48 kHz, and in the spectral wavelength range of 200–950 nm. However, the NO emission lines from the $NO\gamma(A^2\Sigma^+ \rightarrow X^2\Pi_r)$ electronic transitions are the main features of the spectra in the UV region. In the pulsed DBD plasma jet, NO radicals are made through O_2 and N_2 dissociating via the electron collision process [21]. The NO γ band originated from the N_2 metastable state based on the following impact reactions [22, 23]:

Excitation:

$$N_2\left(A^3\Sigma_u^+\right) + NO\left(X^2\Pi\right) \rightarrow N_2\left(X^2\Sigma_g\right) + NO(A^2\Sigma^+)$$

Radiative transition:$NO(A^2\Sigma^+) \rightarrow NO\left(X^2\Pi\right) + hv\ (NO - \gamma band)$

Additionally, the highly reactive radicals, i.e., OH emission band $(A^2\Sigma, v = 0 \rightarrow X^2\Pi, v' = 0)$ are detected at the wavelength of 309 nm. It must be noted that, the OH radicals are generated owing to the presence of water vapor molecules in the environment air [24]. Where, these two different populations of excited state OH could be likely produced via the direct dissociation of the water vapor molecules through the following relation:

$$H_2O + e^- \rightarrow OH\left(A^2\Sigma\right) + H + e^-$$

or based on H_2O^+ species dissociative recombination:

$$H_2O^+ + e^- \rightarrow OH\left(A^2\Sigma\right) + H$$

where H_2O^+ is made by the argon metastables and subsequent dissociative recombination processes [25]. Furthermore, the excited argon neutrals can dissociate H_2O leading to the OH radical production as follows [26]:

$$Ar^* + H_2O \rightarrow OH\left(A^2\Sigma\right) + Ar + H$$

Furthermore, as shown in Fig. 4, the emission spectra between the wavelengths of 300–450 nm are dominated in the presence of second positive system N_2 $(C^3\Pi_u \rightarrow B^3\Pi_g)$, the first positive system $N_2(B^3\Pi_g \rightarrow A^3\Sigma_u^+)$ and the first negative system $N_2^+(B^2\Sigma_u^+ \rightarrow X^2\Sigma_g^+)$. Many excitation processes such as electron collision excitation from the molecular ground state $N_2(X^1\Sigma_g^+)$, the first metastable state $N_2(A^3\Sigma_u^+)$, pooling reaction and transfer of energy between collisional partners would result in these transitions [27, 28].

Moreover, in the nitrogen plasma discharge media, the population of the radiative state N_2 $(C^3\prod_u)$ is resulted from many excitation and quenching processes as follows:

Electron collision excitation process,

$$N_2\left(X^1\Sigma_g^+\right) + e \rightarrow N_2\left(C^3\Pi_u\right) + e$$

$$N_2\left(X^1\Sigma_g^+\right) + e \rightarrow N_2\left(A^3\Sigma_u^+\right) + e$$

first metastable state quenching of the excited states based on the following reactions,

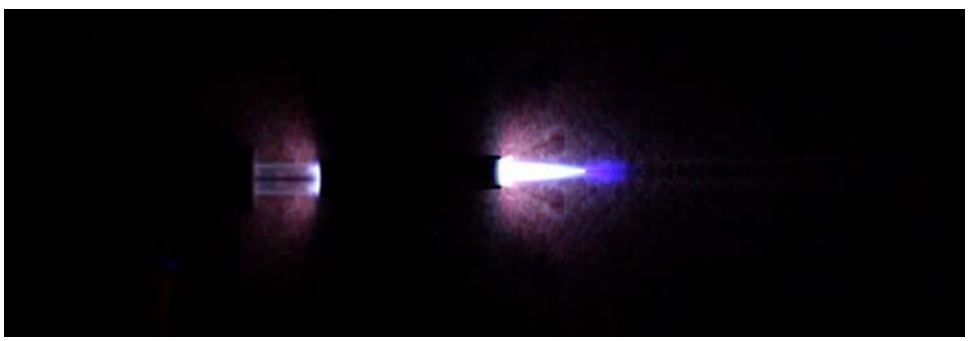

Fig. 3 Photographs of the developed pulsed plasma jet in the operational conditions at 90% of argon in Ar/N_2 mixture

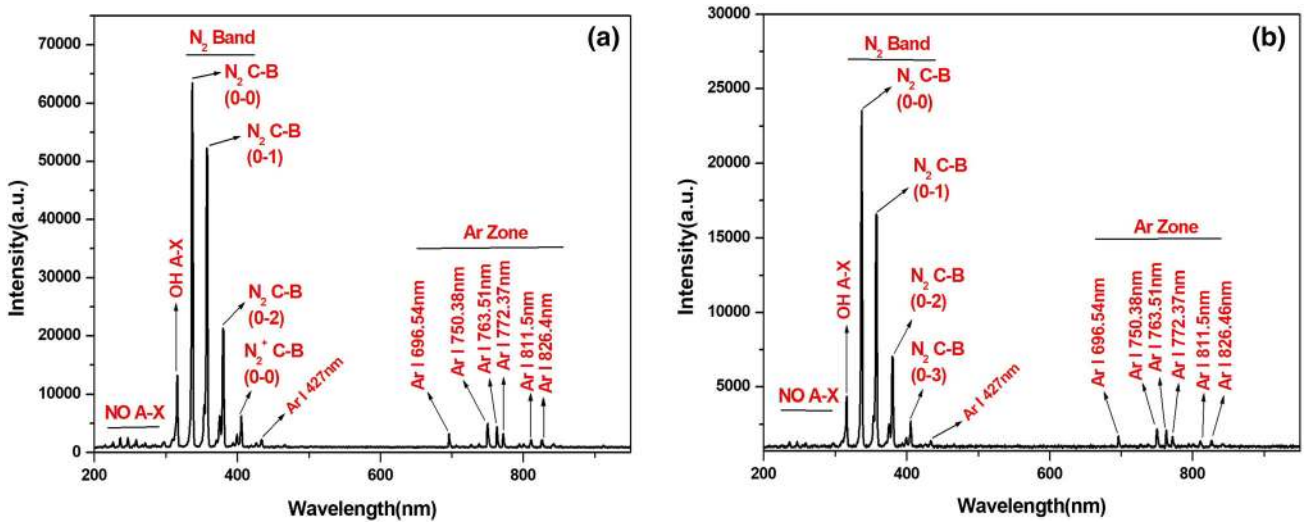

Fig. 4 Typical emission spectra of the developed pulsed plasma jet (corrected for the spectrometer's spectral response) at the applied voltage and frequency of $V = 4.8$ kV, $f = 48$ kHz and, **a** 95%Ar, **b** 75%Ar in the mixture

$$N_2\left(A^3\Sigma_u^+\right) + e \rightarrow N_2\left(C^3\Pi_u\right) + e$$

$$N_2\left(A^3\Pi_u^+\right) + e \rightarrow N_2\left(B^3\Pi_g\right) + e$$

associative excitation as,

$$N_2\left(X^1\Sigma_g^+\right) + N_2\left(A^3\Sigma_u^+\right) \rightarrow N_2\left(C^3\Pi_u\right) + N_2\left(X^1\Sigma_g^+\right)$$

and pooling reactions, transfer of energy between collisional partners and Penning excitation as follows [29–31]:

$$N_2\left(A^3\Sigma_u^+\right) + N_2\left(A^3\Sigma_u^+\right) \rightarrow N_2\left(C^3\Pi_u\right) + N_2(X^1\Sigma_g^+)$$

$$N_2\left(A^3\Sigma_u^+\right) + N_2\left(A^3\Sigma_u^+\right) \rightarrow N_2\left(C^3\Pi_u\right) + N_2(X^1\Sigma_g^+)$$

Moreover, in Ar/N_2 mixture plasma discharges, the population of N_2 $(C^3\Pi_u)$ excited state may originate from the transfer of the internal energy from a metastable level of argon atoms to the ground level of nitrogen molecules [32]. Here, the argon metastable states, i.e., $Ar_m^*(^3P_2,\ ^3P_0)$ play an important role. These metastables have the energies 11.55 and 11.72 eV which are higher than the threshold excitation energy of nitrogen molecule (11.1 eV). Therefore, adding Ar to N_2 plasma discharges leads to increasing of the emission intensities significantly. Hence, the concentration of the active species can be expected by Penning effect based on the following reaction [33]:

$$N_2\left(X^1\Sigma_g^+\right) + Ar_m^*\left(^3P_2,\ ^3P_0\right) \rightarrow N_2\left(C^3\Pi_u\right) + Ar\ (E > 11\,\text{eVfrom}\ N_2(X, v = 0))$$

Moreover, the ground state molecular ions can be made via the Penning ionization by the metastable argon atoms $(^3P_2,\ ^3P_0)$ as follows [34]:

$$N_2\left(X^1\Sigma_g^+\right) + Ar_m^*\left(^3P_2,\ ^3P_0\right) \rightarrow N_2^+\left(X^2\Sigma_g^+\right) + Ar + e$$

The $N_2^+\left(X^2\Sigma_g^+\right)$ state can be further excited to $N_2^+\left(B^2\Sigma_u^+\right)$ radiative state either by electron collision or impact of metastable argon atoms.

The next decaying process of the radiative states gives rise to the photon emission from (0–0) band of the Second Positive System at the wavelength of 336.1 nm:

$$N_2\left(C^3\Pi_u, v' = 0\right) \rightarrow N_2\left(B^3\Pi_g, v'' = 0\right) + hv$$

As a result, the emission intensity of (0–0) band of second positive system is proportional to the population density of N_2 $(C^3\Pi_u)$ level [34, 35].

The $N_2^+\left(B^2\Sigma_u^+\right)$ excited state can be populated either by the direct electron collision excitation from the ground state of the $N_2\left(X^1\Sigma_g^+\right)$ molecule through [21, 34]

$$N_2\left(X^1\Sigma_g^+\right) + e \rightarrow N_2^+\left(B^2\Sigma_u^+\right) + 2e(E > 18.5\,\text{eVfrom}\ N_2(X, v = 0))$$

or based on step by step electron collision ionization of the N_2 molecules and, then, the later electron impact excitation of the molecular ion as follows:

$$N_2\left(X^1\Sigma_g^+\right) + e \rightarrow N_2^+\left(X^2\Sigma_g^+\right) + 2e\ (E > 15.6\,\text{eVfrom}\ N_2(X, v = 0))$$

$$N_2^+\left(X^2\Sigma_g^+\right) + e \rightarrow N_2^+\left(B^2\Sigma_u^+\right) + e\ (E > 3.3\,\text{eVfrom}\ N_2^+(X, v = 0)\text{at}15.6\,\text{eV})$$

The subsequent radiative decays of $N_2^+\left(B^2\Sigma_u^+\right)$ excited state can emit the characteristic photons of (0–0) band of

first negative system at wavelength of 391.4 nm through the following reaction:

$$N_2^+\left(B^2\Sigma_u^+, v'=0\right) \rightarrow N_2^+\left(X^2\Sigma_g^+, v=0\right)+hv$$

The (0–0) band emission intensity of the First Negative System is corresponding to the population of the $N_2^+\left(B^2\Sigma_u^+\right)$ state [21, 34].

The Ar^{+*} excited state can be populated by either one-step process [33]:

$$Ar + e(E > 35\,eV) \rightarrow Ar^{+*}$$

or via the two-step processes as follows:

$$Ar + e(E > 15.5\,eV) \rightarrow Ar^{+}$$

$$Ar^{+} + e(E > 19.5\,eV) \rightarrow Ar^{+*}.$$

It must be noted that, at the low temperature plasma discharges, there are very few electrons which their energies are more than 35 eV. However, these energies are often needed to the simultaneous excitation and ionization processes. Hence, the excitation of the ground state of the plasma discharge ions is mainly performed by the two-step processes. Moreover, the emission intensity from the radiative state of Ar^{+*} provides the necessary data on the ground state ions density Ar^+ [36].

As shown in Fig. 4, argon emission lines intensity appears at the wavelength range of 696.1–911.4 nm, the high intensity peaks corresponding to Ar I peaks are related to the 4*s*–4*p* transition. These peaks are detected at the wavelengths of 696.5 nm, 706.7 nm, 727.3 nm and 738.3 nm; the transition 4*p*–6*s* was appeared at 703.2 nm; the transition 4*s*–4*p* at 750.4 nm; and the transition 4*s*–4*p* at the wavelengths of 763.5 nm and 772.4 nm [21]. The mechanism for exciting of the $2p_1$ level of Ar is the one-step electron collision excitation from the ground state. The peaks due to the N_2 First Positive System are determined at the wavelengths of 632.3, 670.5, 676.4, 678.6, 705.9, 716.5 and 762.7 nm, when N_2 gas is added [37].

In this work, the peaks of excited hydrogen atoms, profiles and H_β spectral emission lines broadening are used. In addition, the plume of developed pulsed DBD plasma jet is produced at atmospheric air (N_2, O_2 and water vapor). Hence, the various emitting species could be detected from the emission spectra of the developed pulsed DBD plasma jet, such as Ar and N excited atoms, also O_2^+, O, NO and OH molecular emission bands. On the other hand, determination of kinetic temperature using the OES method is based on temperature measurements which are obtained from the energy levels of rotationally excited states. Generally, it is assumed that, the kinetic temperature and the rotational temperature of the ground state are in equilibrium. Moreover, the dipole-allowed transition lifetime of the excited levels are applied to characterize the rotational distribution. It must be noted that, this lifetime is much shorter than the collision time [38].

Normally, plasma state is analyzed by the light radiated in the visible region, where the spectral measurements are relatively easy. The rotationally excited molecules frequently execute energy transfer by collision with the other gaseous molecules. As a result, the rotational temperature is approximately equal to the gas temperature. Thus, the gas temperature, T_g, can be specified from the rotational temperature, T_r [39]. Then, the emission spectra of the nitrogen molecule Second Positive System bands are observable. The rotational temperatures can be calculated using the rotational spectrum of N_2^+ at wavelength of 391.44 nm ($B^2\Sigma_u^+ - X^2\Sigma_g^+$ transition), which is used at the high resolutions of the spectrometer. The R-branch between the wavelengths of 389 nm and 391 nm can be exclusively distinguished. The R lines intensities, I_n, are function of the rotational temperature, T_r, as follows [40]:

$$I_R = C^{st}K' \exp\left[-\frac{B'K'(K'+1)hc}{k_B T_R}\right] \tag{4}$$

where C^{st} is a constant and K' are the quantum numbers for the excited state $B^2\Sigma_u^+$; h, c, k_B and B' are Planck constant, speed of light, Boltzmann and rotational constants, respectively. Here, $B'hc/k_B = 2.988K$ with the constants is used. The slope of $\mathrm{Ln}(I/K')$ versus $K'(K'+1)$ gives the rotational temperature. This has been done with the R lines appearing in the wavelength range of 389–391 nm [40].

In this work, the Gardet models are used to obtain the rotational temperature from the emission spectrum of N_2^+ at the wavelength of 391.44 nm. These models are applicable for the low resolutions. In these models, three steps are followed: (1) determination of wavelength positions λ_0, (2) intensity factors calculation, and (3) the so-calculated spectrum convolution with a linear combination of Gaussian and Lorentzian functions $\mathrm{LC}(\lambda)$ which must be used to describe rightly the apparatus function [41].

The number of molecules that are excited into a given vibrational state is assessed by the vibrational quantum number v. Moreover, it is proportional to the vibrational energy (E_v) by the Boltzmann law to $\exp(-E_v/k_BT)$. The vibrational band intensity is written as follows [40]:

$$I_{v',v''} = \mathrm{const.}\nu^4 A(v'v'')e^{-\frac{E_{v'}}{k_B T}} \tag{5}$$

where v', v'' is the vibrational quantum number of upper and lower states, respectively. $A(v'v'')$ is the transition probability (can be found in tables and it corresponds to the electron vibration state functions overlap), and ν is wavenumber (mainly wavenumber of the band head). The expression for vibrational band intensity shows that the plot of $\mathrm{Ln}(I_{v'v''}/\nu^4 A(v'v''))$ versus $E_{v'}$ must be linear. Thus,

the vibrational temperature can be calculated from the slope of this straight line [40].

Figure 5 shows a typical Boltzmann plot of the relative intensity distributions. Considering the scattered data points and fitting errors, the vibrational temperature, T_{vib}, is estimated about 4150 K at the applied voltage and frequency of 408 kV, 48 kHz and 95% of argon percentage in the Ar/N_2 mixture. The vibrational temperature (T_{vib}) of the pulsed plasma jet is determined by the Boltzmann plot method. Three $N_2(C^3\Pi_u \rightarrow B^3\Pi_g)$ vibrational bands, $\Delta v = -1(0-1, 1-2, 2-3)$, $\Delta v = -2(0-2, 1-3, 2-4)$, and $\Delta v = -3(0-3, 1-4, 2-5)$ are chosen to obtain T_{vib}. The wavelengths of 349.9, 353.6, 357.6, 370.9, 375.4, 380.4, 394.2, 399.7, 405.8 nm are considered for each $N_2(C^3\Pi_u \rightarrow B^3\Pi_g)$ vibrational transition. The other parameters have taken from ref. no. [42].

It is worthwhile to mention that there are many emission lines which are related to the excited argon atom. They have reliable transition probabilities that are already published in the existing literature. Supposing that the upper levels of the selected atomic transitions are in the PLTE conditions, the usual Boltzmann plot technique can be applied to calculate the excitation temperature in the plume of the developed pulsed DBD plasma jet. Hence, the following relation defines the relative transition probabilities for two different emission lines [43, 44]:

$$\ln\left(\frac{I\lambda_{ul}}{A_{ul}g_u}\right) = \ln\left(\frac{hcN_0}{4\pi U(T)}\right) - \frac{E_u}{kT_{exc}} \quad (6)$$

where I, A_{ul}, g_u, λ_{ul}, E_u and k denote the total intensity, transition probability, degeneracy of the upper level, wavelength, excitation energy and the Boltzmann constant, respectively. However, the model assumes that the electron collisions with excited atoms are dominant in the populating and depopulating of the excited atoms.

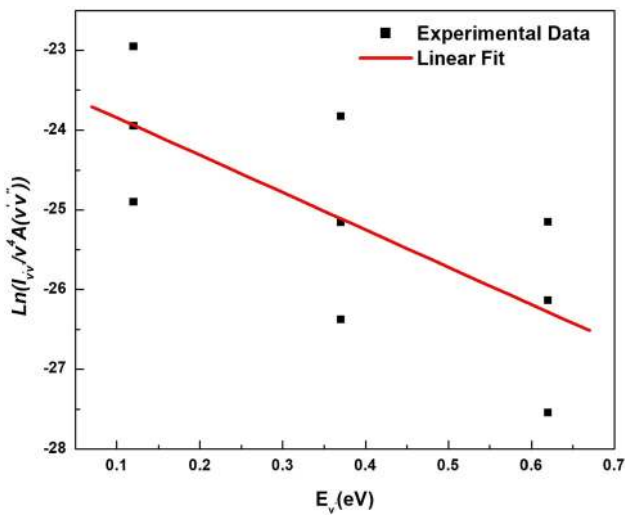

Fig. 5 Typical Boltzmann plot of $N_2(C^3\prod_u \rightarrow B^3\prod_g)$ vibrational distribution with the vibrational temperature of $T_{vib} = 4150$ K

Figures 6 shows the rotational, vibrational, and excitation temperatures of the designed pulsed plasma jet as a function of the applied voltage and frequency of pulsed power supply at different Ar percentages in the Ar/N_2 mixtures. Since $T_{exc} > T_{vib} > T_{rot}$, regardless of the experimental conditions, the plasma source operates in the non-equilibrium conditions. As seen, at the higher voltages and frequencies, all the temperatures are increased. This is owing to the fact that, at the higher applied voltages, owing to the higher electric fields in the discharge medium, the number of high energy electrons in the tail of EEDF will increase. Indeed, the Penning ionization including the argon metastable species is enhanced. Moreover, the rotational temperature increase at the higher Ar contributions in the mixture. It must be noted that, the ionization cross sections and potentials for the molecular nitrogen ($\sim 2.5 \times 10^{-20} m^2$ and $\sim$ 15.7 eV) are almost close to the argon atom [45, 47]. Hence, illustration of the observed increase in electron temperature in Ar/N_2 mixture is not easy. However, the increase in the rotational temperature at the higher argon amounts in the mixture might be owing to the Electron Energy Distribution Functions (EEDFs) difference and its direct influences on the higher secondary electron efficiency at the target. Moreover, in the formed plasma discharge by the Ar/N_2 gaseous mixture, the lifetime of absorbing species $Ar(1s_5)$ is longer than the emitting species $N_2(B^3\Pi_g)$. Therefore, in comparison with $N_2(B^3\Pi_g)$ molecules, $Ar(1s_5)$ metastable species can diffuse farther away from the plasma discharge medium. Thus, their temperature reduces. For Ar/N_2 gaseous mixtures, the corresponding values for the First Positive System are almost similar. As a result, the higher argon contribution in the mixture will not significantly affect the gas temperature. On the other hand, the story for the Second Positive System is quite different. Indeed, an efficient energy transfer between the nitrogen ground state and Ar metastable atoms could involve strong overpopulation of rotational emission lines. Hence, the rotational temperatures are much larger than the obtained temperatures from the First Positive System.

Furthermore, Fig. 6 shows the increasing of the vibrational temperature of N_2 Second Positive System in the plasma mixture Ar/N_2 at the higher argon contributions. It shows that in Ar/N_2 gas mixture plasma, there is a high excitation transfer of N_2 from argon metastable Ar_m^* through the following reaction [46]:

$$Ar_m^* + N_2(X) \rightarrow Ar(^1S_0) + N_2(C)$$

where $N_2(X)$ and $Ar(^1S_0)$ are the ground states of nitrogen and argon, respectively. Moreover, the electron impacts

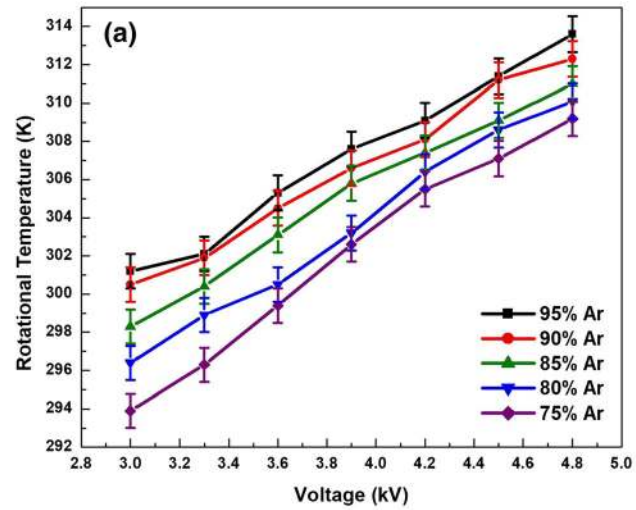
(a)
Rotational Temperature (K)
Voltage (kV)
95% Ar
90% Ar
85% Ar
80% Ar
75% Ar

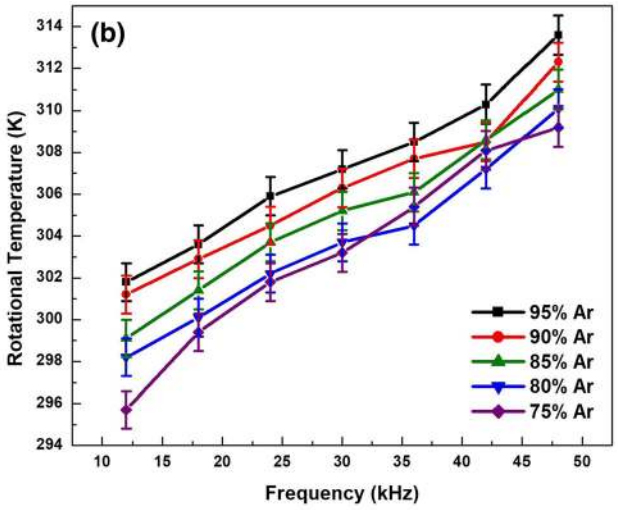
(b)
Rotational Temperature (K)
Frequency (kHz)
95% Ar
90% Ar
85% Ar
80% Ar
75% Ar

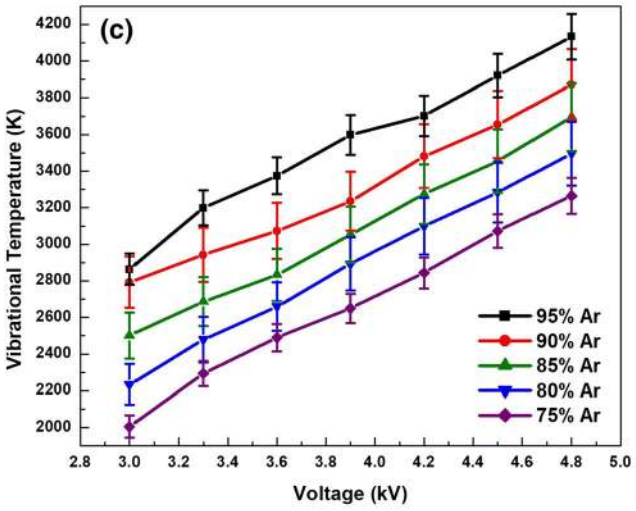
(c)
Vibrational Temperature (K)
Voltage (kV)
95% Ar
90% Ar
85% Ar
80% Ar
75% Ar

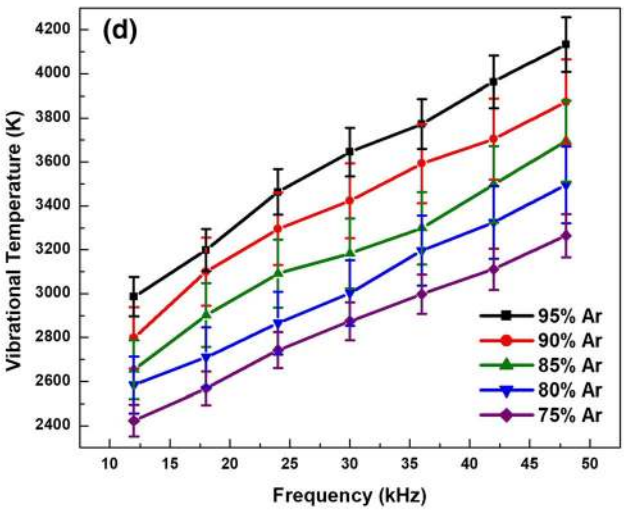
(d)
Vibrational Temperature (K)
Frequency (kHz)
95% Ar
90% Ar
85% Ar
80% Ar
75% Ar

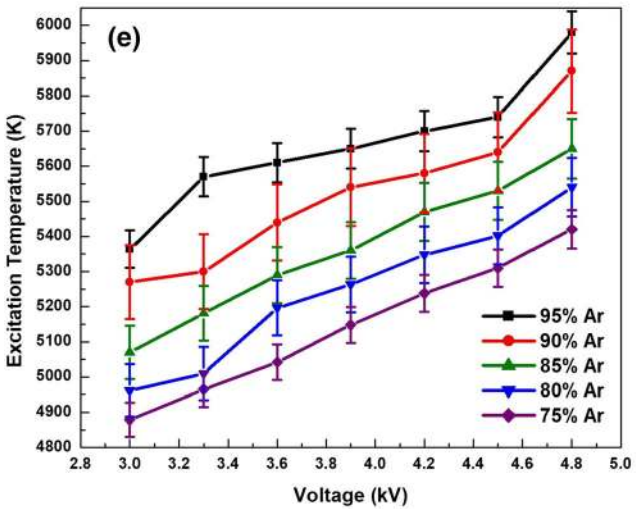
(e)
Excitation Temperature (K)
Voltage (kV)
95% Ar
90% Ar
85% Ar
80% Ar
75% Ar

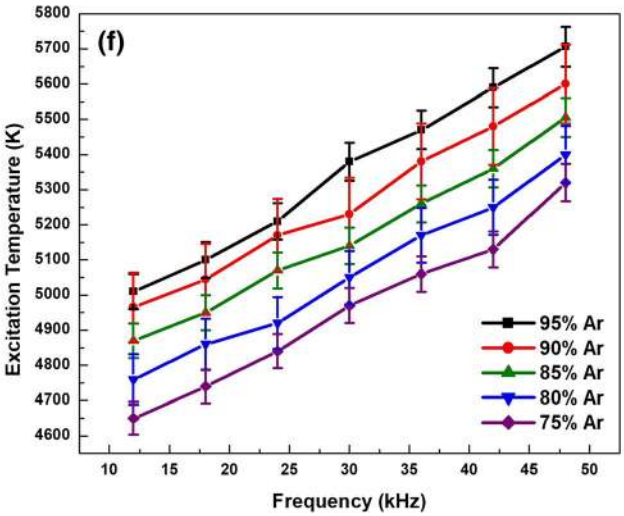
(f)
Excitation Temperature (K)
Frequency (kHz)
95% Ar
90% Ar
85% Ar
80% Ar
75% Ar

◀**Fig. 6** Evolution of (**a** [with error bar from up to down ± 0.1, ± 0.17, ± 0.23, ± 0.19, ± 14], **b** [with error bar up to down ± 0.21, ± 0.27, ± 0.18, ± 0.15, ± 0.11]) the rotational temperature, (**c** [with error bar from up to down ± 0.13, ± 0.08, ± 0.11, ± 0.15, ± 0.12], **d** [with error bar from up to down ± 0.11, ± 0.14, ± 0.17, ± 0.13, ± 0.1]) vibrational temperature and (**e** [with error bar from up to down ± 0.19, ± 0.16, ± 0.12, ± 0.0.2, ± 0.17], **f** [with error bar from up to down ± 0.21, ± 0.14, ± 0.11, ± 0.18, ± 0.15]) excitation temperature as function of applied voltage and frequency of pulsed power source, respectively

and pooling reactions between the nitrogen metastable states must be considered [47]. However, all these processes contribute to the increase of vibrational temperature at the higher argon percentages in Ar/N_2 gas mixture.

Similar to the performed calculations for the vibrational temperature, a Boltzmann plot based on the Eq. (3) can be applied to drive the excitation temperatures from the slope fittings. In this case, the $\ln(I\lambda_{ul}/A_{ul}g_u)$ is plotted versus the upper level electronic energy (E_u) for the selected emission lines of Ar I. The atomic parameters of Ar I emission lines are taken from the National Institute of Standards and Technology (NIST) database [48]. As shown in Fig. 6, the electron temperature increases at the higher Ar amounts in Ar/N_2 gaseous mixture. This might be corresponding to the lower electron collision cross section of argon atoms compared with the nitrogen molecules. Thus, the plasma electrons will have enough time to get accelerated by the electric field. Consequently, the kinetic energy of electrons will be increased. These energetic electrons can excite and ionize the nitrogen molecules or generate the argon metastable states. The formed argon metastables will successively collide with N_2 molecules and excite or ionize them. This is owing to the Penning ionization and excitation events which lead to the formation of atomic argon neutral ground states and excitation and ionization of N_2 species in the plasma discharge medium of pulsed plasma jet.

It must be mentioned that the streamer corona, transient spark and micro-discharges produce the cold and non-equilibrium plasma discharges with the temperatures between 300 and 550 K. Besides, the glow discharge plasmas are hotter and still in the non-equilibrium conditions (1900 K). On the other hand, the microwave plasma discharges are much hotter with the temperatures between 3000 and 4000 K. Moreover, the vibrational temperature always remains higher than the rotational one. Thus, it shows that the plasma is in the PLTE condition. Furthermore, the conditions for the vibrational temperatures (2500–3500 K) govern transient spark and glow discharges. However, the rotational temperatures are higher for both the transient spark and glow discharges [56]. Moreover, as seen in Fig. 6 for the designed pulse plasma jet, the rotational and vibrational temperatures are about 360–1000 K at the applied voltage of 7 kV. Hence, the developed pulsed plasma jet is suitable for the sterilization applications [49]. In addition, in a typical experimental setup, Britun et al. used a thin wire electrode as anode which was placed over a planar cathode with the spatial distance of 500 μm between the powered electrodes. The rotational and vibrational temperatures were obtained at about 1200 and 5000 K, respectively [50].

Generally, the Stark broadening analysis of the spectral profile for the H_β emission line, which is emitted by the plasma discharge, is the most common procedure to obtain the electron density, n_e [51–53]. Based on the selection rules for the hydrogen atomic transitions [54], the allowed transitions (multipletes) are related to the H_β emission lines that are between $2p$–$4s$, $2s$–$4p$ and $2p$–$4d$ energy levels. It must be noted that several broadening mechanisms influence the emission line-shapes in plasma discharge media [55, 56]. They are mainly including the natural broadening (this is usually not important), Doppler broadening, pressure broadening and Stark broadening [51]. The Stark broadening, $\Delta\lambda_S$, can be directly related to the electron density in plasma discharge. Hence, it can be used to determine the plasma density, n_e. The hydrogen Balmer series (H_β) is usually used to obtain the plasma electron density without considering the fine structure of the emission lines and plasma ions dynamics [55, 57]. On the other hand, the Full-Width at Half-Maximum (FWHM) is used to determine the broadened emission line profile. Then, the FWHM broadening values of the Stark broadening that may affect the H_β line can be obtained. The FWHM of Stark broadening is related to the electron density as follows [58]:

$$\Delta\lambda_{\text{stark}} = 2 \times 10^{-11}(n_e^{2/3}) \tag{7}$$

Thus, Stark broadening can be used to compute the electron density. Where the plasma electron density is in the cm^{-3} [58]. Stark broadening at wavelength of 486.1 nm is considered for H_β. Moreover, the Stark broadening is related to Lorentz and van der Waals broadenings through the following relation [59]:

$$\Delta\lambda_{\text{Lorentz}} = \Delta\lambda_{\text{stark}} + \Delta\lambda_{\text{van der waals}}. \tag{8}$$

Finally, the pressure broadening is resulted from the energy levels perturbation of the emitting atoms in the presence of surrounding neutral species. It is worthy to mention that the pressure broadening leads to a Lorentzian profile. Moreover, it can be subdivided into the resonance and van der Waals (vdw) broadenings. The resonance broadening occurs when the emitters and perturbers are similar or the upper or the lower state of the detected emission line is in a resonance level. On the other hand, the

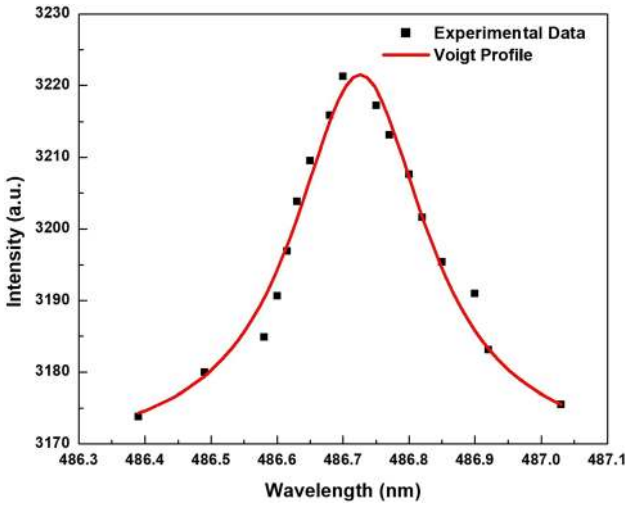

Fig. 7 Comparison of experimental data and Voigt profile with $\Delta\lambda_L = 0.246$ and $\Delta\lambda_G = 0.189$ nm

van der Waals (vdw) broadening takes place when the emitters are perturbed by the neutral species of a foreign gas. In this work, the density of H atoms was extremely low. Hence, the only van der Waals broadening is taken into the account. Thus, the FWHM of the vdw profile is written as follows [59, 60]:

$$\Delta\lambda_{\text{vanderWaals}} = 3.6 \times \frac{P}{T^{0.7}} \tag{9}$$

where p is the pressure in atmosphere and, T is the gas temperature in Kelvin which is almost equal to the rotational temperature.

Generally, the Lorentz broadening can be found through the fitting of experimental spectra with Voigt profile which is the superposition of Gauss and Lorentz broadenings. Here, the fitting process is performed using the Origin software and Lorentzian FWHM. Hence, using the Lorentz and van der Waals broadenings, the Stark broadening is calculated. Then, the plasma electron density is obtained. Figure 7 shows the Lorentz broadening which is calculated via fitting of the experimental spectra to the Voigt profile ($\Delta\lambda_{\text{Lorentz}} = 0.246$nm). Inserting the gas pressure of 1 atm, temperature of 312 K and %95 of argon presence in the Ar/N_2, the van der Waals broadening is calculated as $\Delta\lambda_{\text{vavderWaals}} = 0.122$ nm. Then, the Stark broadening would be 0.124 nm corresponding to the electron density of $n_e = 4.91 \times 10^{14}\text{cm}^{-3}$.

The variations of electron number density as a function of applied voltage and frequency of the pulsed power source at the various Ar contributions in Ar/N_2 mixture are shown in Fig. 8. As seen, the electron number density grows with the applied impulse voltage and frequency. However, this is owing to the fact that, at the higher voltages and frequencies, the input power to the discharge medium of the pulse plasma jet is higher. This reflects in the higher electric fields and, consequently, the ionization rate of neutral Ar atoms and N_2 molecules is increased. Furthermore, the electron number density reduces at the higher Ar percentages in the mixture. As a result, the electron number density reduction will reflect in the decreasing of the dissociation rate of N_2. Indeed, at the higher Ar percentages in the mixture, the probability of production of Ar metastable species will increase. Thus, the generation rate of $N_2(C^3\prod_u)$ is enhanced. This is the reason behind the reduction of the spectral emission intensity at the higher Ar percentages in the mixture. Additionally, this phenomenon shows the molecular dissociation reduction.

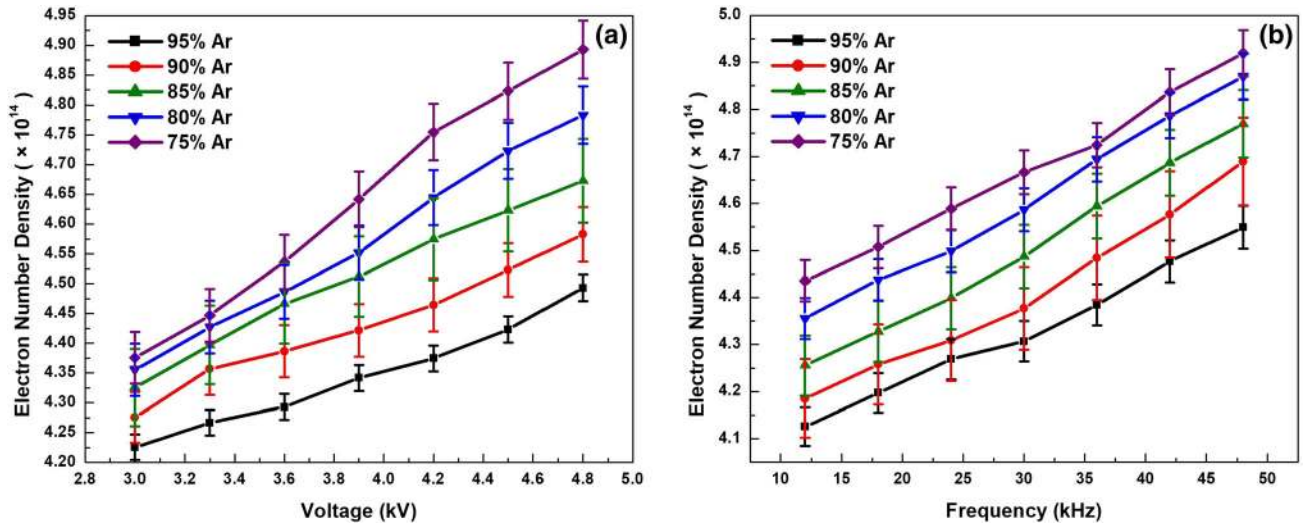

Fig. 8 The plasma electron density as a function of applied impulse, **a** voltage [with error bar from up to down ± 0.25, ± 0.29, ± 0.32, ± 0.27, ± 0.3] and **b** frequency [with error bar up to down ± 0.22, ± 0.3, ± 0.25, ± 0.28, ± 0.32] at the various percentages of Ar in Ar/N_2 mixture

Conclusions

In this work, the obtained optical emission spectra from the excited atomic Ar and molecular N_2 in the plasma discharge medium of a developed atmospheric pressure pulsed DBD plasma jet are examined. The argon contribution in the Ar/N_2 mixture is varied from 75 to 95% and, the temperatures and density of different species in the plasma discharge medium of the designed pulsed plasma jet are obtained. In the operational working conditions of the pulsed plasma jet, the highest emission intensities of the first stages for argon ionization (Ar I) are recorded in the wavelength range of 696–912 nm. It was observed that, at the wavelength of 750.38 nm, the radiation intensity of Ar ($4p_0 \rightarrow 4s_1$) transitions at the 95% of Ar in Ar/N_2 mixture is higher. On the other hand, increasing of the Ar percentage results in the higher emission intensities from N_2 molecules. It was found that, for all the argon percentages in the mixture, the plasma electron density and all the temperatures will increase with the applied impulse voltage and frequency. Besides, while all the measured temperatures are increased at the higher argon contributions, the electron number density is decreased.

References

1. Shenton, M.J., Stevens, G.C.: Surface modification of polymer surfaces: atmospheric plasma versus vacuum plasma treatments. J. Phys. D Appl. Phys. **34**, 2761 (2001)
2. Huang, W.T., Li, S.Z.: Preliminary study on applications of an atmospheric-pressure argon plasma discharge with a single-electrode configuration. IEEE Trans. Plasma Sci. **38**, 121 (2010)
3. Abramzon, N., Joaquin, J.C., Bray, J., Brelles-Mariño, G.: Biofilm destruction by RF high-pressure cold plasma jet. IEEE Trans. Plasma Sci. **34**, 1304 (2006)
4. Deng, X., Shi, J., Kong, M.G.: Physical mechanisms of inactivation of Bacillus subtilis spores using cold atmospheric plasmas. IEEE Trans. Plasma Sci. **34**, 1310 (2006)
5. Czerwiec, T., Greer, F., Graves, D.B.: Nitrogen dissociation in a low pressure cylindrical ICP discharge studied by actinometry and mass spectrometry. J. Phys. D Appl. Phys. **38**, 4278–4289 (2005)
6. Laroussi, M., Lu, X.: Room-temperature atmospheric pressure plasma plume for biomedical applications. Appl. Phys. Lett. **87**, 902 (2005)
7. Shao, T., Zhang, C., Long, K., Zhang, D., Wang, J., Yan, P., Zhou, Y.: Surface modification of polyimide films using unipolar nanosecond-pulse DBD in atmospheric air. Appl. Surf. Sci. **12**, 3888 (2010)
8. Tao, S., Yang, Y., Cheng, Z., Hui, J., Ping, Y., Yuanxiang, Z.: Generation of atmospheric pressure plasma by repetitive nanosecond pulses in air using water electrodes. Plasma Sci. Technol. **13**, 735 (2011)
9. Tao, S., Cheng, Z., Zheng, N., Yang, Y., Ping, Y., Yuanxiang, Z.: Nanosecond repetitively pulsed dielectric barrier discharge in air at atmospheric pressure. Plasma Sci. Technol. **13**, 591 (2011)
10. Lieberman, M.A., Lichtenberg, A.J.: Principles of plasma discharges and materials processing. Wiley, Hoboken, NJ (2005)
11. Foster, K.W., Moy, R.L., Fincher, E.F.: Advances in plasma skin regeneration. J. Cosmet. Dermatol. **7**, 169 (2008)
12. Khan, F.U., Rehman, N.U., Naseer, S., Naveed, M.A., Qayyum, A., Khattak, N.A., Zakaullah, M.: Diagnostic of 13.56 MHz RF sustained Ar-N2 plasma by optical emission spectroscopy. Eur. Phys. J. Appl. Phys. **45**, 11002 (2009)
13. Qayyum, A., Zeb, S., Naveed, M.A., Rehman, N.U., Ghauri, S.A., Zakaullah, M.: Optical emission spectroscopy of Ar–N2 mixture plasma. J. Quant. Spectrosc. Radiat. Transfer **107**, 361 (2007)
14. Bousquet, A., Spinelle, L., Cellier, J., Tomasella, E.: Optical emission spectroscopy analysis of Ar/N2 plasma in reactive magnetron sputtering. Plasma Process. Polym. **6**, S605 (2009)
15. Kilinov, A., Veis, P., Foissac, C., Dupret, C., Supiot, P.: Spectroscopic Characterization of Nitrogen–Argon Discharge Created by Helical Cavity. WDS'07. In: Proceedings of contributed papers. Part II, p 175 (2007)
16. Ohata, M.: Spectroscopic characteristic and analytical capability of Ar–N2 Inductively coupled plasma in axially viewing optical emission spectrometry. Anal. Sci. **32**, 219 (2016)
17. Doronin, Y.S., Libin, M.Y., Samovarov, V.N., Vakula, V.L.: Spectroscopic observation of (N2) 2 dimers in free icosahedral N2 and Ar-N2 clusters. Phys. Rev. A **84**, 023201 (2011)
18. Tendero, C., Tixier, C., Tristant, P., Desmaison, J., Leprince, P.: Atmospheric pressure plasmas: a review. Spectrochim. Acta. B. **61**, 2–30 (2006)
19. Calzada, M.D., Rodero, A., Sola, A., Gamero, A.: Excitation kinetic in an argon plasma column produced by a surface wave at atmospheric pressure. J. Phys. Soc. Jpn. **65**, 948–954 (1996)
20. Fujimoto, T., McWhirter, R.W.P.: Validity criteria for local thermodynamic equilibrium in plasma spectroscopy. Phys. Rev. A **42**, 6588 (1990)
21. Norlén, G.: Wavelengths and energy levels of Ar I and Ar II based on new interferometric measurements in the region 3400–9800 Å. Phys. Scr. **8**, 249–268 (1973)
22. Shimizu, K., Oda, T.: Emission spectrometry for discharge plasma diagnosis. Sci. Technol. Adv. Mater. **2**, 577–585 (2001)
23. Piper, L.G., Cowles, L.M., Rawlins, W.T.: State-to-state excitation of NO (A $2\Sigma^+$, $v' = 0, 1, 2$) by N2 (A $3\Sigma^+$ u, $v' = 0, 1, 2$). J. Chem. Phys. **85**, 3369–3378 (1986)
24. Machala, Z., Morvová, M., Marode, E., Morva, I.: Removal of cyclohexanone in transition electric discharges at atmospheric pressure. J. Phys. D Appl. Phys. **33**, 3198–3213 (2000)
25. Bruggeman, P., Iza, F., Guns, P., Lauwers, D., Kong, M.G., Gonzalvo, Y.A., Leys, C., Schram, D.C.: Electronic quenching of OH (A) by water in atmospheric pressure plasmas and its influence on the gas temperature determination by OH (A–X) emission. Plasma Sources Sci. Technol. **19**, 015016 (2009)
26. Nie, D., Wang, W., Yang, D., Shi, H., Huo, Y., Dai, L.: Optical study of diffuse bi-directional nanosecond pulsed dielectric barrier discharge in nitrogen. Spectrochim. Acta Part A **79**, 1896–1903 (2011)
27. Sakamoto, T., Matsuura, H., Akatsuka, H.: Spectroscopic study on the vibrational populations of N2CΠ3 and BΠ3 states in a microwave nitrogen discharge. J. Appl. Phys. **2**, 023307 (2007)
28. Wang, D., Zhao, D., Feng, K., Zhang, X., Liu, D., Yang, S.: The cold and atmospheric-pressure air surface barrier discharge

plasma for large-area sterilization applications. Appl. Phys. Lett. **16**, 161501 (2011)
29. Bibinov, N.K., Fateev, A.A., Wiesemann, K.: On the influence of metastable reactions on rotational temperatures in dielectric barrier discharges in He–N2 mixtures. J. Phys. D Appl. Phys. **34**, 1819 (2001)
30. Petitjean, L., Ricard, A.: Emission spectroscopy study of N2-H2 glow discharge for metal surface nitriding. J. Phys. D Appl. Phys. **17**, 919 (1984)
31. Qayyum, A., Zeb, S., Ali, S., Waheed, A., Zakaullah, M.: Optical emission spectroscopy of abnormal glow region in nitrogen plasma. Plasma Chem. Plasma Process. **25**, 551 (2005)
32. Bockel, S., Amorim, J., Baravian, G., Ricard, A., Stratil, P.: A spectroscopic study of active species in DC and HF flowing discharges in-and Ar–mixtures. Plasma Sources Sci. Technol. **5**, 567 (1996)
33. Sugimoto, I., Nakano, S., Kuwano, H.: Enhanced saturation of sputtered amorphous SiN film frameworks using He-and Ne-Penning effects. J. Appl. Phys. **75**, 7710 (1994)
34. Popa, S.D.: Influence of pressure on spectral intensities in a flowing nitrogen glow discharge. J. Phys. D Appl. Phys. **29**, 416 (1996)
35. Behringer, K., Fantz, U.: Spectroscopic diagnostics of glow discharge plasmas with non-Maxwellian electron energy distributions. J. Phys. D Appl. Phys. **27**, 2128 (1994)
36. Donnelly, V.M.: Plasma electron temperatures and electron energy distributions measured by trace rare gases optical emission spectroscopy. J. Phys. D Appl. Phys. **37**, R217 (2004)
37. Boffard, J.B., Lin, C.C., DeJoseph Jr., C.A.: Application of excitation cross sections to optical plasma diagnostics. J. Phys. D Appl. Phys. **37**, R143 (2004)
38. Schmiedt, L., Kaňka, A., Hrachová, V.: Optical emission spectroscopy—passive method for plasma diagnostics in DC glow oxygen discharge, WDS'07. In: Proceedings of contributed papers: part II—physics of plasmas and ionized media, Prague, 3–6 June, p 20–24 (2008)
39. Haraki, N., Nakano, S., Ono, S., Teii, S.: Oxygen radical density measurement in O2–N2 gas mixture plasma by means of a thin platinum wire. Elect. Eng. Jpn. **149**, 14–20 (2004)
40. Herzberg, G.: Molecular Spectra and Molecular Structure I: Spectra of Diatomic Molecules. Van Nostrand, New York (1950)
41. Gardet, G., Moulard, G., Courbon, M., Rogemond, F., Druetta, M.: Evaluation of the rotational temperature in N2 discharges using low-resolution spectroscopy. Meas. Sci. Technol. **11**, 333–341 (2000)
42. Shemansky, D.E., Broadfoot, A.L.: Excitation of N2 and $N2^+$ systems by electrons—I. Absolute transition probabilities. J. Quant. Spectrosc. Radiat. Transf. **10**, 1385–1400 (1971)
43. Stoffels, E., Flikweert, A.J., Stoffels, W.W., Kroesen, G.M.: Plasma needle: a non-destructive atmospheric plasma source for fine surface treatment of (bio) materials. Plasma Sources Sci. Technol. **11**, 383 (2002)
44. Pandhija, S., Rai, A.K.: In situ multielemental monitoring in coral skeleton by CF-LIBS. Appl. Phys. B **94**, 545 (2009)
45. Raju, G.G.: Collision cross sections in gaseous electronics part I: what do they mean? IEEE Electr. Insul. Mag. **22**, 5 (2006)
46. Winicur, D.H., Fraites, J.L.: Electronic-energy exchange cross sections for Ar*(3 P) and N 2 (X 1 Σ g+). J. Chem. Phys. **61**, 1548 (1974)
47. Levaton, J., Amorim, J., Franco, D.: Experimental and calculated N (4S) temporal density profile in the N2 flowing post-discharge. J. Phys. D Appl. Phys. **38**, 2204 (2005)
48. National Institute of Standards and Technology 1979-2008 NIST: Atomic Spectra Data Base (Gaithersburg, MD: NIST Physics Laboratory) and http://physics.nist.gov/PhysRefData/ASD
49. Seo, Y.S., Mohamed, A.A., Woo, K.C., Lee, H.W., Lee, J.K., Kim, K.T.: Comparative studies of atmospheric pressure plasma characteristics between He and Ar working gases for sterilization. IEEE Trans. Plasma Sci. **38**, 2954–2962 (2010)
50. Britun, N., Gaillard, M., Ricard, A., Kim, Y.M., Kim, K.S., Han, J.G.: Determination of the vibrational, rotational and electron temperatures in N_2 and Ar–N_2 rf discharge. J. Phys. D Appl. Phys. **40**, 1022 (2007)
51. Griem, H.R.: Plasma spectroscopy. McGraw-Hill, New York (1964)
52. Torres, J., Van Sande, D.E., Sande, M.J., Van der Mullen, J.J., Gamero, A., Sola, A.: Stark broadening for simultaneous diagnostics of the electron density and temperature in atmospheric microwave discharges. Spectrochim. Acta B. **61**, 58 (2006)
53. Laux, C.O., Spence, T.G., Kruger, C.H., Zare, R.N.: Optical diagnostics of atmospheric pressure air plasmas. Plasma Sources Sci. Technol. **12**, 125 (2003)
54. Eisberg, R., Resnick, R.: Quantum Physics of Atoms, Molecule, Solids, Nuclei and Particles. Elsevier, Rio de Janeiro (1979)
55. Iza, F., Lee, J.K.: Particle-in-cell simulations of planar and cylindrical Langmuir probes: floating potential and ion saturation current. J. Vac. Sci. Technol. **24**, 1366 (2006)
56. Machala, Z., Janda, M., Hensel, K., Jedlovský, I., Leštinská, L., Foltin, V., Martišovitš, V., Morvova, M.: Emission spectroscopy of atmospheric pressure plasmas for bio-medical and environmental applications. J. Mol. Spectrosc. **243**, 194–201 (2007)
57. Nikiforov, A.Y., Leys, C., Gonzalez, M.A., Walsh, J.L.: Electron density measurement in atmospheric pressure plasma jets: stark broadening of hydrogenated and non-hydrogenated lines. Plasma Sources Sci. Technol. **24**, 034001 (2015)
58. Qian, M., Ren, C., Wang, D., Zhang, J., Wei, G.: Stark broadening measurement of the electron density in an atmospheric pressure argon plasma jet with double-power electrodes. J. Appl. Phys. **107**, 063303 (2010)
59. Belostotskiy, S.G., Ouk, T., Donnelly, V.M., Economou, D.J., Sadeghi, N.: Gas temperature and electron density profiles in an argon dc microdischarge measured by optical emission spectroscopy. J. Appl. Phys. **107**, 053305 (2010)
60. Mehr, F.J., Biondi, M.A.: Electron-temperature dependence of electron-ion recombination in Argon. Phys. Rev. **176**, 322 (1968)

Publisher's Note